



Published in final edited form as:

*Proc IEEE Int Symp Biomed Imaging*. 2018 April ; 2018: 743–746. doi:10.1109/ISBI.2018.8363680.

## TOWARDS OPTIMAL LINEAR ESTIMATION OF ORIENTATION DISTRIBUTION FUNCTIONS WITH ARBITRARILY SAMPLED DIFFUSION MRI DATA

Divya Varadarajan and Justin P. Haldar

Signal and Image Processing Institute, University of Southern California, Los Angeles, CA 90089

### Abstract

The estimation of orientation distribution functions (ODFs) from diffusion MRI data is an important step in diffusion tractography, but existing estimation methods often depend on signal modeling assumptions that are violated by real data, lack theoretical characterization, and/or are only applicable to a small range of q-space sampling patterns. As a result, existing ODF estimation methods may be suboptimal. In this work, we propose a novel ODF estimation approach that learns a linear ODF estimator from training data. The training set contains ideal data samples paired with corresponding ideal ODFs, and the learning procedure reduces to a simple linear least-squares problem. This approach can accommodate arbitrary q-space sampling schemes, can be characterized theoretically, and is theoretically demonstrated to generalize far beyond the training set. The proposed approach is evaluated with simulated and *in vivo* diffusion data, where it is demonstrated to outperform common alternatives.

### 1. INTRODUCTION

The ability to infer fiber orientations from diffusion MRI (dMRI) data enables noninvasive *in vivo* mapping of important biological fiber pathways (a process known as diffusion tractography) [1], which in turn can provide important information for clinical applications and basic scientific research. While many methods have been proposed to estimate orientation information from dMRI, existing approaches suffer from a number of limitations. On one hand, model-based estimation approaches like diffusion tensor imaging (DTI) [2] and constrained spherical deconvolution (CSD) [3] are widely used and can work well, but rely on strong modeling assumptions that are known to be violated in real tissues. The behavior of such model-based methods in the presence of model violations is still an active area of research [4], although there is substantial evidence to suggest that there are scenarios in which modeling violations yield substantial performance degradations. On the other hand, there also exist “model-free” methods like those based on 3D-SHORE [5, 6] and GQI [7] that make much fewer assumptions, and are therefore more immune to modeling violations. However, while these methods have also been demonstrated to perform well, there is still no existing theory or empirical evidence to suggest that such approaches are actually close to optimal within the universe of all possible orientation estimators.

Our present work is based on the hypothesis that existing orientation estimation methods are suboptimal. This hypothesis is inspired by a general theoretical framework we recently

introduced [8] that provides unique theory-driven performance characterizations of linear estimators. Specifically, our previous theoretical analysis suggests that the angular resolution and noise sensitivity of existing linear estimation approaches may not actually be close to achieving what is theoretically possible within the class of linear estimators. These types of theoretical characterizations have never previously been available in dMRI (except in narrowly-defined special cases [9, 10]), and we believe they have the potential to enable substantial progress towards optimal linear estimator design.

In this work, we investigate a new theory-inspired approach to linear orientation estimator design. This new approach, which we call ERFO (EAP Response Function Optimized ODF estimation), makes use of machine learning principles to construct a linear orientation distribution function (ODF) estimator based on training data. This approach is quite general, can be used with arbitrary q-space sampling schemes, and can be tailored to a range of different dMRI application contexts. In addition, our focus on linear estimators distinguishes our approach from previous learning-based approaches which use nonlinear estimation [11–13]. While nonlinear estimators have the potential to outperform linear estimators, the “black box” nature of most learning methods can make it hard to predict whether a learned nonlinear estimator will still perform well in imaging contexts that it hasn’t been specifically trained on. In contrast, the learned ERFO estimators are linear, which allows “model-free” and training-independent theoretical characterization of estimator performance and ensures good behavior and generalizability.

## 2. BACKGROUND

### 2.1. Orientation Distribution Functions

Under the standard q-space model of dMRI, the measured diffusion signal  $E(\mathbf{q})$  at q-space location  $\mathbf{q}$  is related to the ensemble average propagator (EAP)  $P(\mathbf{r})$  through the Fourier transform relationship:

$$E(\mathbf{q}) = C \int P_{\Delta}(\mathbf{r}) e^{-i2\pi\mathbf{q}^T \mathbf{r}} d\mathbf{r} + Cn(\mathbf{q}), \quad (1)$$

where  $n(\mathbf{q})$  denotes noise (which we assume to be independent homoscedastic random variables with variance  $\sigma^2$  and zero mean) and  $C$  denotes an arbitrary scaling constant (we assume data normalization such that  $C = 1$ ). The EAP is a probability distribution summarizing the statistical characteristics of water diffusion within a macroscopic voxel. Since the orientation-dependent characteristics of the EAP are usually of primary concern in tractography applications, the EAP is frequently marginalized to an ODF by radial integration:

$$O(\mathbf{u}) = \frac{1}{2} \int_{-\infty}^{\infty} P_{\Delta}(\alpha\mathbf{u}) \alpha^2 d\alpha \quad (2)$$

where orientation is specified by the unit vector  $\mathbf{u}$ . The one-dimensional integral from Eq. (2) can also be expressed as a three-dimensional integral by invoking Dirac delta functions:

$$O(\mathbf{u}) = \int P_{\Delta}(\mathbf{r})g^*(\mathbf{u}, \mathbf{r})d\mathbf{r}, \text{ with } g^*(\mathbf{u}, \mathbf{r}) \triangleq |\mathbf{r}^T \mathbf{u}|^2 \delta\left(\sqrt{\|\mathbf{r}\|^2} - |\mathbf{r}^T \mathbf{u}|\right). \quad (3)$$

The significance of this 3D integral representation will be explained when we discuss theoretical characteristics of ERFO.

## 2.2. Linear ODF Estimation

Linear ODF estimation methods can all be represented in the following form:

$$\hat{O}(\mathbf{u}) = \sum_{m=1}^M a_m(\mathbf{u})E(\mathbf{q}_m), \quad (4)$$

where  $\hat{O}(\mathbf{u})$  is the ODF estimate as a function of the orientation  $\mathbf{u}$ , we have assumed a finite number  $M$  of q-space measurements,  $E(\mathbf{q}_m)$  is the noisy q-space data measured at location  $\mathbf{q}_m$ , and  $a_m(\mathbf{u})$ ,  $m = 1, \dots, M$  are the coefficients that fully specify the linear ODF estimation method.

Our previous work [8] derived a direct theoretical relationship between the estimated ODF and the true EAP:

$$\hat{O}(\mathbf{u}) = \int P_{\Delta}(\mathbf{r})g(\mathbf{u}, \mathbf{r})d\mathbf{r} + \sum_{m=1}^M a_m(\mathbf{u})n(\mathbf{q}_m), \text{ with } g(\mathbf{u}, \mathbf{r}) \triangleq \sum_{m=1}^M a_m(\mathbf{u}) \cos(2\pi\mathbf{q}_m^T \mathbf{r}). \quad (5)$$

Equation (5) has two components, one that depends on the true EAP but is independent of the noise, and another that depends on the noise but is independent of the true EAP. The function  $g(\mathbf{u}, \mathbf{r})$  that interacts with the true EAP is termed the EAP response function (ERF), and can be used to infer the accuracy and resolution characteristics of a given linear estimator [8]. The noise term appearing in Eq. (5) also allows us to predict the variance of  $\hat{O}(\mathbf{u})$  assuming that we know the noise variance characteristics of  $n(\mathbf{q}_m)$  [8].

## 3. ERFO

### 3.1. Estimator Design Formulation

The ERFO estimator is designed based on pairs of ideal noiseless data and the corresponding ideal noiseless ODFs. Specifically, assuming that we are given  $P$  such training pairs  $\{O_p(\mathbf{u}), E_p(\mathbf{q})\}_{p=1}^P$ , as well as the q-space sampling locations  $\{\mathbf{q}_m\}_{m=1}^M$  and the noise variance  $\sigma^2$ , we optimize the vector of ERFO estimation coefficients  $\mathbf{a}(\mathbf{u}) = [a_1(\mathbf{u}) \dots a_M(\mathbf{u})]^T$  by minimizing (with respect to  $\mathbf{a}(\mathbf{u})$ ) the following minimum mean-squared error loss function:

$$\sum_{p=1}^P \mathbb{E} \left[ \left| O_p(\mathbf{u}) - \sum_{m=1}^M a_m(\mathbf{u}) (E_p(\mathbf{q}_m) + n(\mathbf{q}_m)) \right|^2 \right], \quad (6)$$

where  $\mathbb{E}$  is used to denote statistical expectation with respect to the noise samples. Under our noise assumptions, it can be shown [8] that minimizing Eq. (6) is equivalent to minimizing

$$\sum_{p=1}^P \left| O_p(\mathbf{u}) - \sum_{m=1}^M a_m(\mathbf{u}) E_p(\mathbf{q}_m) \right|^2 + P\sigma^2 \sum_{m=1}^M |a_m(\mathbf{u})|^2. \quad (7)$$

The two terms in this loss function are easy to interpret: the first term represents the estimator bias that would be obtained from noiseless data, while the second term represents the expected contribution to the mean-squared error resulting from noise. Minimization of Eq. (7) can be represented as a simple linear-least squares problem for each  $\mathbf{u}$  value, which can be easily solved using standard matrix inversion techniques.

At first glance, the connection between our ERFO estimator and the ERF-based theoretical characterization from [8] may not be immediately apparent. This connection is formalized in the following subsection.

### 3.2. Theoretical Characteristics

Let  $P_{\Delta}^{(p)}(\mathbf{r})$  denote the original EAP that is associated with the training pair  $O_p(\mathbf{u})$  and  $E_p(\mathbf{q})$ . In this case, simple manipulations suggest that the first term (describing estimator bias) from Eq. (7) can be rewritten in terms of EAPs/ERFs as

$$\sum_{p=1}^P \left| O_p(\mathbf{u}) - \sum_{m=1}^M a_m(\mathbf{u}) E_p(\mathbf{q}_m) \right|^2 = \sum_{p=1}^P \left| \int P_{\Delta}^{(p)}(\mathbf{r}) (g^*(\mathbf{u}, \mathbf{r}) - g(\mathbf{u}, \mathbf{r})) d\mathbf{r} \right|^2. \quad (8)$$

When expressed in this form, it becomes apparent that the bias term from the ERFO cost function can roughly be interpreted as encouraging minimal error between the optimized ERF  $g(\mathbf{u}, \mathbf{r})$  and the ideal response function  $g^*(\mathbf{u}, \mathbf{r})$  from Eq. (3), while the training samples are used to define an  $\mathbf{r}$ -dependent weighting function on this error. In particular, this weighting can be roughly viewed as encouraging strong correspondence between  $g(\mathbf{u}, \mathbf{r})$  and  $g^*(\mathbf{u}, \mathbf{r})$  in regions where  $P_{\Delta}^{(p)}(\mathbf{r})$  is large, while not being very sensitive to large ERF errors in regions where  $P_{\Delta}^{(p)}(\mathbf{r})$  is small.

This interpretation is useful because, while we might not know the exact EAP model or training data that is appropriate for a given application, the ERF provides a model-independent approach that allows us to predict the general behavior of the resulting estimator. Moreover, the training model only serves as a weighting of the ERF error that

implicitly provides information about where the most informative information about the true EAP is located, and we do not expect this to change very much under realistic variations in the underlying model. As a result, while we will almost certainly train ERFO with an imperfect model, the estimator we end up with should still be expected to have desirable theoretical characteristics and generalization capabilities.

#### 4. EVALUATION

To evaluate our proposed approach and demonstrate its flexibility with respect to the q-space sampling protocol, we designed ERFO estimators for two different q-space sampling protocols: 1) the single-shell 64-direction uniform sampling protocol (b-value =  $3000\text{s/mm}^2$ ) from [7], and 2) the 288-sample multishell protocol used by the human connectome project [4]. We used the DTI model with different choices of orientations and eigenvalues to generate ideal noiseless training pairs, and training was performed assuming SNR=35.

Figure 1 compares the ERFs obtained with ERFO against ERFs obtained with other linear estimators (FRACT [10] and 3D-SHORE [5, 6]). The theoretical characterizations suggest that in the single shell case, ERFO has a similar (but very slightly worse) ERF mainlobe width than FRACT ( $13\ \mu\text{m}$  for ERFO versus  $12.2\ \mu\text{m}$  for FRACT), though also has substantially better ERF sidelobe characteristics (29% for ERFO versus 37% for FRACT). The ERF mainlobe width is expected to correlate with angular resolution, while the ERF sidelobe level is expected to be associated with undesirable signal leakage and false positive/false negative orientation detections [8]. As a result, we can reasonably expect ERFO to outperform FRACT in this case. In the multishell case, ERFO has a substantially better mainlobe width than 3D-SHORE ( $13.7\ \mu\text{m}$  for ERFO versus  $16.7\ \mu\text{m}$  for 3D-SHORE) at the expense of moderately worse sidelobe characteristics (30% for ERFO versus 18% for 3D-SHORE). As before, we can reasonably expect ERFO to outperform 3D-SHORE.

We next tested ERFO empirically using numerical simulations. We simulated the signal that would be observed from water diffusing in two infinitely-long cylinders crossing at various angles (between  $30 - 90^\circ$ ) and with different diffusivity/anisotropy values in the physiological range, with SNR=35. We then used this data to reconstruct ODFs (or fiber orientation distributions in the case of CSD) with ERFO, CSD [3], and FRACT [10] for the single-shell protocol, and using ERFO and 3D-SHORE [5, 6] for the multishell protocol. The single fiber response function needed for the model-based CSD approach was estimated in two different ways. In one case, the single fiber response function was estimated from the white matter near the left postcentral gyrus (PG) in an *in vivo* dataset, while the other case estimated the single fiber response function from white matter in the corpus callosum (CC). We quantitatively evaluated errors with respect to the ground truth using both the location of the estimated ODF peaks and the normalized root mean-squared error (NRMSE).

The results of these simulations are shown in Fig. 2. In the single shell case, we observe that ERFO has lower errors than CSD and FRACT, and that the performance of CSD is dependent on the white matter model that was chosen. In the multishell case, ERFO has lower errors than 3D-SHORE.

We also applied ERFO to the *in vivo* single-shell 64-sample NTU brain dataset from [7]. Representative reconstructed ODFs are shown in Fig. 3 from a region of the brain with three crossing fiber structures (the cortico-spinal tract, fibers originating from the corpus callosum, and the superior longitudinal fasciculus). The results show that ERFO and CSD are successful at estimating the orientation corresponding to the superior longitudinal fasciculus, while FRACT has difficulties resolving this orientation. Comparing ERFO and CSD, this orientation is represented more prominently in the ERFO reconstructions. Tractography results from a seed place in this same region of interest are shown in Fig. 4. While we don't know ground truth, we believe that the ERFO results seem less noisy and have much better correspondence with the expected anatomy compared to the alternatives.

## 5. CONCLUSION

We have presented and evaluated ERFO, a novel learning-based method for designing linear ODF estimation methods from dMRI data acquired with arbitrary q-space sampling. The resulting estimators are shown to perform well in practice, and have nice theoretical characteristics that ensure they will generalize to cases they haven't been trained for. Our theoretical, numerical simulation, and *in vivo* evaluations all suggest that ERFO has substantial performance advantages compared to several popular ODF estimators.

## Acknowledgments

This work was supported in part by research grants NSF CCF-1350563, NIH R21 EB022951, NIH R01 NS074980, and NIH R01 NS089212.

Some of the computation for the work described in this paper was supported by the University of Southern California's Center for High-Performance Computing ([hpc.usc.edu](http://hpc.usc.edu)).

## 6. REFERENCES

1. Jeurissen B, Descoteaux M, Mori S, and Leemans A, "Diffusion MRI fiber tractography of the brain," NMR Biomed, 2017.
2. Basser PJ and Jones DK, "Diffusion tensor MRI: theory, experimental design and data analysis - a technical review," NMR Biomed, vol. 15, pp. 456–467, 2002. [PubMed: 12489095]
3. Tournier J-D, Calamante F, and Connelly A, "Robust determination of the fibre orientation distribution in diffusion MRI: Non-negativity constrained super-resolved spherical deconvolution," NeuroImage, vol. 35, pp. 1459–1472, 2007. [PubMed: 17379540]
4. Sotiropoulos SN et al., "Advances in diffusion MRI acquisition and processing in the human connectome project," NeuroImage, vol. 80, pp. 125–143, 2013. [PubMed: 23702418]
5. Ozarslan E, Koay CG, Shepherd TM, Komlosh ME, Irfanoglu MO, Pierpaoli C, and Basser PJ, "Mean apparent propagator (MAP) MRI: A novel diffusion imaging method for mapping tissue microstructure," NeuroImage, vol. 78, pp. 16–32, 2013. [PubMed: 23587694]
6. Merlet SL and Deriche R, "Continuous diffusion signal, EAP and ODF estimation via compressive sensing in diffusion MRI," Med. Image Anal, vol. 17, pp. 556–572, 2013. [PubMed: 23602920]
7. Yeh F-C, Wedeen VJ, and Tseng W-YI, "Generalized q-sampling imaging," IEEE Trans. Med. Imag, vol. 29, pp. 1626–1635, 2010.
8. Varadarajan D and Haldar JP, "A theoretical signal processing framework for linear diffusion MRI: Implications for parameter estimation and experiment design," NeuroImage, vol. 161, pp. 206–218, 2017. [PubMed: 28830765]
9. Tuch DS, "Q-ball imaging," Magn. Reson. Med, vol. 52, pp. 1358–1372, 2004. [PubMed: 15562495]

10. Haldar JP and Leahy RM, "Linear transforms for Fourier data on the sphere: Application to high angular resolution diffusion MRI of the brain," *NeuroImage*, vol. 71, pp. 233–247, 2013. [PubMed: 23353603]
11. Golkov V, Dosovitskiy A, Sperl JI, Menzel MI, Czisch M, Samann P, Brox T, and Cremers D, "q-space deep learning: Twelve-fold shorter and model-free diffusion MRI scans," *IEEE Trans. Med. Imag.*, vol. 35, pp. 1344–1351, 2016.
12. Koppers S and Merhof D, "Direct estimation of fiber orientations using deep learning in diffusion imaging," in *MLMI*, 2016, pp. 53–60.
13. Ye C and Prince JL, "Fiber orientation estimation guided by a deep network," in *MICCAI*, 2017, pp. 575–583. [PubMed: 28944347]

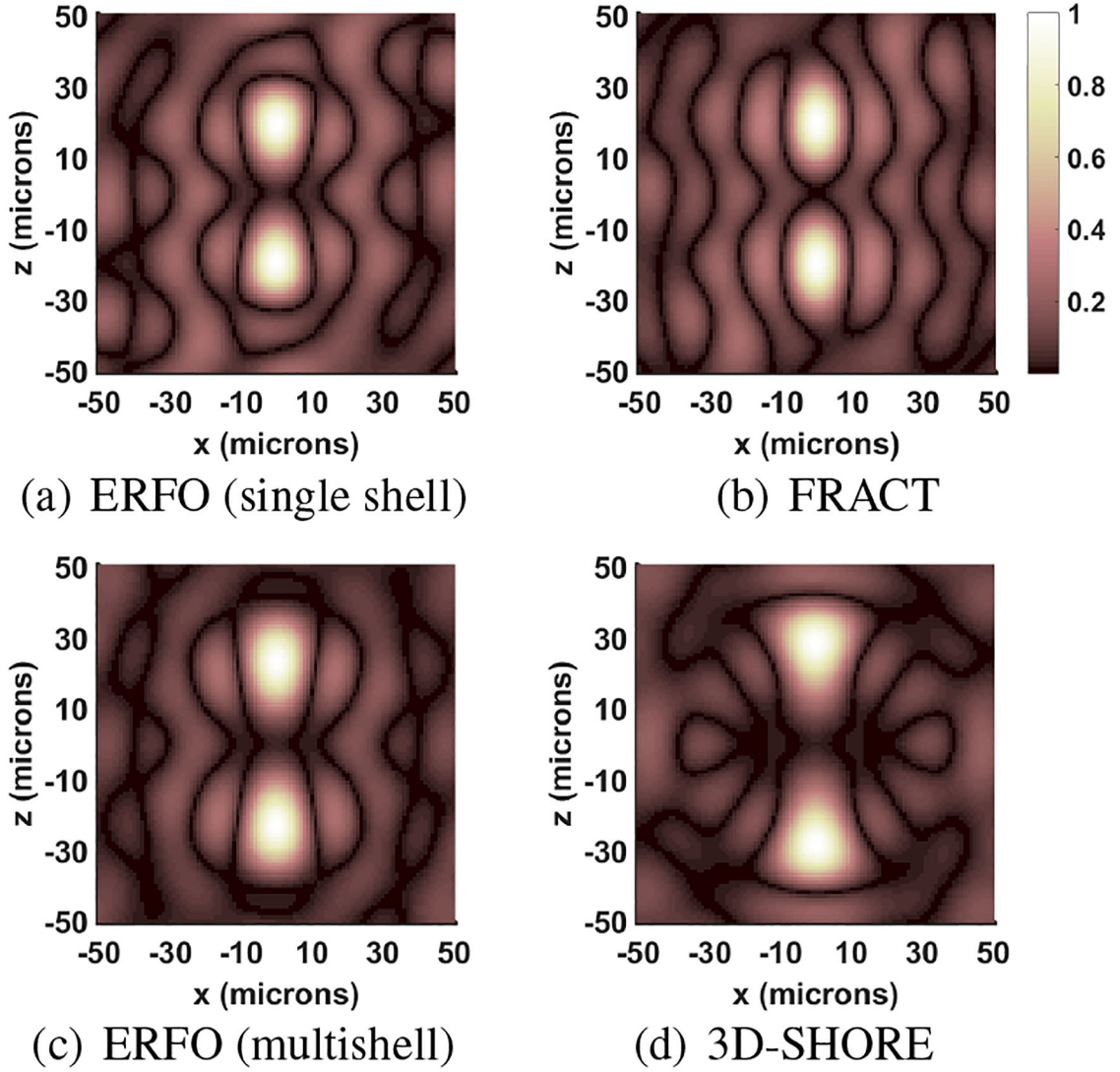


**Fig. 1:** ERFs for (a,b) single shell and (c,d) multishell acquisition for (a,c) ERFO, (b) FRACT, and (d) 3D-SHORE. See [8] for description of our ERF display conventions.

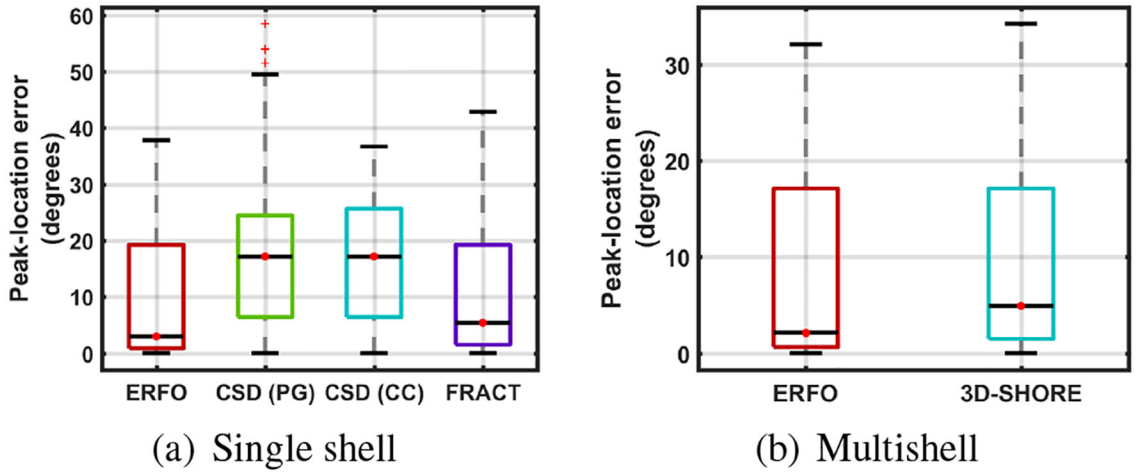


**Fig. 2:** Comparison of orientation estimation errors for (a) single shell and (b) multishell numerical simulations.

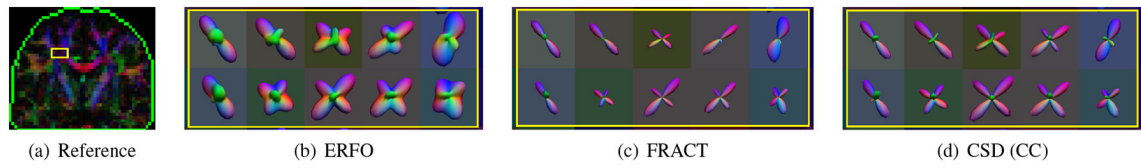


**Fig. 3:** Estimated ODFs using different estimation methods from a region-of-interest that is marked in (a).

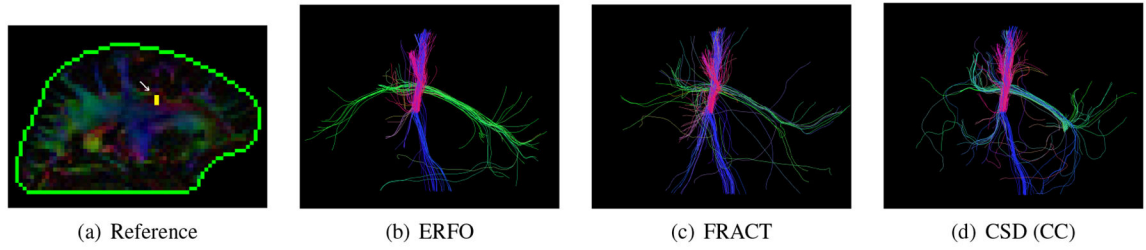


**Fig. 4:**  
Tractography results corresponding to the different ODF estimation methods shown in Fig. 3.